



B-MASTER: Scalable Bayesian Multivariate Regression Analysis for Selecting Targeted Essential Regressors to Identify the Key Genera in Microbiome-Metabolite Relation Dynamics

Priyam Das *

Department of Biostatistics, Virginia Commonwealth University

Tanujit Dey 

Center for Surgery and Public Health, Brigham and Women's Hospital,
Harvard Medical School

Christine B. Peterson 

Department of Biostatistics, The University of Texas MD Anderson Cancer Center

and

Sounak Chakraborty 

Department of Statistics, University of Missouri

December 10, 2024

Abstract

The gut microbiome significantly influences responses to cancer therapies, including immunotherapies, primarily through its impact on the metabolome. Despite some existing studies addressing the effects of specific microbial genera on individual metabolites, there is little to no prior work focused on identifying the key microbiome components at the genus level that shape the overall metabolome profile. To bridge this gap, we introduce B-MASTER (Bayesian Multivariate regression Analysis for Selecting Targeted Essential Regressors), a fully Bayesian framework incorporating an l_1 penalty to promote sparsity in the coefficient matrix and an l_2 penalty to shrink coefficients for non-major covariate components simultaneously, thereby isolating essential regressors. The method is complemented with a scalable Gibbs sampling algorithm, whose computational speed increases linearly with the number of parameters and remains largely unaffected by sample size and data-specific characteristics for

*corresponding author; das4@vcu.edu

models of fixed dimensions. Notably, B-MASTER achieves full posterior inference for models with up to four million parameters within a practical time-frame. Using this approach, we identify key microbial genera influencing the overall metabolite profile, conduct an in-depth analysis of their effects on the most abundant metabolites, and investigate metabolites differentially abundant in colorectal cancer patients. These results provide foundational insights into the impact of the microbiome at the genus level on metabolite profiles relevant to cancer, a relationship that remains largely unexplored in the existing literature.

Keywords: Bayesian penalized regression, Gibbs sampling, scalable high-dimensional models, microbiome-metabolites dynamics, colorectal cancer.

1 Introduction

Advances in sequencing technologies and bioinformatic methods have provided new insights on the role of the microbiome in cancer as well as many other diseases that often involve gut health (Xu & Knight 2015). Characterizing how microbiome communities interact with their host, respond to their environment, and influence disease is critical to understanding their role in human health (Lederberg & McCray 2001, Li 2015). Microbiome research is widely used in studies on the cause and mechanism of colorectal (Garrett 2015, Feng et al. 2015) and oral cancer (Wang & Ganly 2017). Advancements in high-throughput sequencing have enabled researchers to analyze the microbiome in much greater detail, which enabled accurate characterization of microbial communities by assessing their richness (the number of different species present), diversity (the variation among species), and abundance (the population sizes of each species) (Huse et al. 2008, Caporaso et al. 2011, Shokralla et al. 2012). These high-throughput sequencing technologies have enabled us to create a detailed profile of the microbial ecosystem and enhanced our understanding of the interaction between microbial colonies in our body with environment, dietary, and other lifestyle choices (Xia & Sun 2017). In particular, by identifying specific microbial patterns linked to diseases, researchers can develop targeted probiotics, prebiotics, and dietary interventions to restore healthy microbial balance. Additionally, microbiome profiling could one day enable personalized medical treatments, tailoring therapies based on an individual's unique microbial composition to improve outcomes for conditions such as cancer, autoimmune disorders, and metabolic syndromes (Belkaid & Hand 2014, Jobin 2018).

The primary mechanism for the impact of the microbiome on human health is through metabolic activity; integrative studies of the microbiome and metabolome have therefore been advocated as a key step forward in understanding host-microbiome interactions (Visconti et al. 2019). The abundances of metabolites, including lipids, amino acids, and other small molecules, can be quantified using mass spectrometry-based metabolomic profiling. Metabolites produced by the microbiome play a key role in shaping immune response and driving inflammation, and are closely linked to immune-related disorders such as inflammatory bowel disease (Yang & Cong 2021). There is also strong evidence that the microbiome creates a microenvironment in the gut that is conducive to cancer formation through the production of detrimental metabolites such as those generated by gut microbes during the

breakdown of red meat (Zhang et al. 2021).

Therefore, it is crucial to understand how gut microbiome components influence metabolites, which are relatively well-studied in the context of cancer progression. Several studies have sought to identify microbial genera that influence specific sets of metabolite components in various contexts, including host metabolism (Davar & Zarour 2022), metabolic disorders (Parker et al. 2020), modulation of short-chain fatty acids (Zhang et al. 2023), amino acid metabolism (Lu et al. 2024), carbohydrate fermentation, and fiber degradation (Song et al. 2022). Although these studies have explored links between genera and metabolites related to specific metabolic functions of interest, there is limited literature addressing how key microbiome components regulate the overall metabolite profile rather than focusing on specific pathway-related activities. Furthermore, while some studies have examined the relationship between microbial families and cancer through their modulation of metabolites (Constantin et al. 2024), to the best of our knowledge, no existing work has investigated associations between microbial genera and differentially abundant metabolites in cancer versus control populations.

In this study, we aim to identify microbiome features that influence downstream metabolic pathway activity, recognizing that metabolically active microbes are often linked to multiple downstream metabolites (Visconti et al. 2019). By leveraging this relationship, we focus on identifying a sparse set of key microbiome features, thereby reducing noise and minimizing false positives by excluding features associated with zero or only a few metabolites. Furthermore, we extend this analysis to identify microbial genera positively or negatively associated with colorectal cancer by examining their influence on differentially abundant metabolite pathways. This approach builds on recent findings on metabolite sets implicated in colorectal cancer as described by Yachida et al. (2019). To achieve these objectives, we comprehensively review the literature on variable selection methods across frequentist and Bayesian frameworks, aiming to design a robust and scalable variable selection strategy aligned with our model presumptions and requirements of analysis.

In the domain of variable selection, some of the most fundamental works can be traced back to Ridge regression (Hoerl & Kennard 1970), the Least Absolute Shrinkage and Selection Operator (LASSO) (Tibshirani 1996), followed by the development of the Elastic-Net penalty (Zou & Hastie 2005). The conceptual frameworks behind these methods revolutionized the field of variable selection, inspiring numerous experts to extend and generalize these

ideas through modifications and adaptations to different model frameworks as needed. Notable extensions include the group Lasso (Yuan & Lin 2006) and adaptive Lasso (Zou 2006). Building upon these foundations, several sparse regression techniques have emerged within the Bayesian domain, often addressing limitations of their frequentist counterparts. Examples include Bayesian Lasso (Park & Casella 2008), Bayesian Group Lasso (Xu & Ghosh 2015), and the Spike-and-Slab Lasso (Rockova & George 2018), among others. As the era of big data unfolded, particularly within the fields of biostatistics and biomedical informatics, literature on sparse regression techniques evolved to incorporate enhanced scalability and tailored adjustments to specific cases (Qian et al. 2020). As time progressed, some of these variable selection techniques were extended to multivariate response regression, both in the frequentist and Bayesian frameworks. Deng et al. (2024) and Li et al. (2015) proposed techniques for multivariate response regression in the frequentist setup, with the latter further extending the method to induce an additional penalty at the group level on the set of predictors. Liquet et al. (2017) extended Bayesian group Lasso for multivariate response regression. Other multivariate extensions, including those based on Spike-and-Slab Lasso (Deshpande et al. 2019) and reduced rank regression (Goh et al. 2017, Chakraborty et al. 2020), have also been explored. Notably, while these methods contribute to understanding the sparse dependence structure between multivariate responses and predictor variables, their underlying mechanisms do not incorporate a penalty mechanism for eliminating non-essential regressors. As such, these methods remain unsuitable for our intended case study, which aims to uncover the key genera involved in microbiome-metabolite relationship dynamics. Furthermore, some of these techniques have been observed to lack scalability at higher dimensions, rendering them infeasible for our case study (further discussed in Section 3).

In order to select the key contributors of the independent covariates influencing the dependent variable cohort, one may draw upon the fundamental mechanisms of Lasso and Ridge regressions, particularly the nature of the shrinkage effects induced by the l_1 and l_2 penalties, and modify them for the relevant context accordingly. The l_1 penalty has been extensively shown to induce sparsity by setting coefficients of less relevant predictors exactly to zero. Whereas, the l_2 penalty induces shrinkage on the overall magnitude of the regression coefficients, which has the potential to reduce the coefficients of targeted predictor components to zero, when applied appropriately (Xu & Ghosh 2015). Therefore,

by incorporating a l_1 penalty on the individual elements of the coefficient vector, alongside an l_2 penalty on the coefficient vectors corresponding to individual regressors, it is possible to induce an overall sparse structure while simultaneously encouraging the shrinkage of entire regressor-specific coefficient vectors. This combination of l_1 and l_2 penalties in the aforementioned targeted manner enables the identification of the key regressors that most significantly influence the response variables. Although this approach was previously explored in a frequentist setup (Peng et al. 2010), it was found to suffer from substantial scalability issues (further explored in Section 3), rendering it inadequate for moderate to high-dimensional settings, including the case study considered in this paper.

In this paper, we reformulate the combination of l_1 and l_2 penalties entirely within the Bayesian framework, which we refer to as Bayesian Multivariate regression Analysis for Selecting Targeted Essential Regressor (B-MASTER). By carefully selecting a hierarchical prior structure for the model, the posterior sampling process is efficiently reduced to a fast and scalable Gibbs sampling algorithm. This makes B-MASTER a superior and more natural choice compared to the corresponding frequentist counterpart, particularly for addressing the following challenges:

1. **Automatic tuning:** B-MASTER incorporates a prior on the tuning parameters, allowing it to adaptively adjust the tuning based on the dataset. However, in a likelihood maximization-based approach, performing cross-validation over two tuning parameters can be computationally intensive. This challenge is particularly pronounced in multivariate response settings, where an increase in the number of predictors as well as response variables exacerbates the computational burden. These issues are examined in detail in Section 3.
2. **Dispersion measures:** B-MASTER simultaneously estimates both the mean and the standard errors of the regression coefficients directly from posterior samples. This contrasts with the frequentist approach, where the estimation procedure does not provide uncertainty measures for the coefficients. While one might consider using the bootstrap method to obtain standard error estimates, the computational challenges inherent in the frequentist approach, as described earlier, make the bootstrap method impractical outside very low-dimensional settings. Specifically, generating bootstrap estimates for standard errors can be nearly impossible within a reasonable timeframe

due to the existing computational constraints.

- 3. Robust and predictable computation time:** The computation time for B-MASTER remains nearly invariant with respect to sample size and across different datasets for a fixed number of parameters. In contrast, the frequentist analogue approach considered in Peng et al. (2010) exhibits substantial fluctuation in computation times across datasets with similar-dimensional parameter spaces. Furthermore, for this approach, computation times are observed to increase as the sample size grows, unlike B-MASTER.
- 4. Scalability in higher-dimensions:** Accompanied by the full Gibbs sampling mechanism for posterior sample generation, B-MASTER remains highly scalable, even in very high-dimensional settings that exceed the dimensions of the dataset considered in this study, as further explored later in the paper. Additionally, the computation time for B-MASTER is highly predictable based on the number of variables, making it particularly suitable for ultra-high-dimensional applications. This predictability allows users to plan ahead for cluster arrangements based on the estimated computational time derived from the number of variables. In contrast, the frequentist approach failed to produce results for the considered dataset within a reasonable time-frame.

The rest of this paper is organized as follows. In Section 2, we introduce the B-MASTER model, providing the full Bayesian formulation and a detailed, step-by-step Gibbs sampling algorithm for model fitting. In Section 3, we demonstrate the effectiveness of the proposed B-MASTER model through several simulated datasets. Section 4 applies B-MASTER to identify “master predictors” for gut microbiota in regulating the microbiome-metabolite dependence structure, based on colorectal cancer data (Yachida et al. 2019). Finally, Section 5 offers a discussion of our conclusions and potential directions for future research.

2 B-MASTER

2.1 Background

Suppose we have N observations with the data described as $(\mathbf{x}^i, \mathbf{y}^i)$ for $i = 1, \dots, N$, where $\mathbf{x}^i = (x_1^i, \dots, x_P^i)$ is a $1 \times P$ vector of predictors and $\mathbf{y}^i = (y_1^i, \dots, y_Q^i)$ is a $1 \times Q$ vector of responses for the i -th observation. We consider the multivariate regression model for multivariate response vector as,

$$\mathbf{y}^i = \mathbf{x}^i \mathbf{B} + \boldsymbol{\epsilon}^i, \quad i = 1, \dots, N, \quad (1)$$

where $\boldsymbol{\epsilon}^i$ is the vector of error terms for the i -th observation, and $\boldsymbol{\epsilon}^i \stackrel{i.i.d.}{\sim} N_Q(\mathbf{0}, \text{diag}(\sigma_1^2, \dots, \sigma_Q^2))$ for $i = 1, \dots, N$. Here, $\mathbf{B} = (\beta_{pq})$ denotes the $P \times Q$ matrix of regression coefficients. In our case study, we aim to identify the key components of the microbiome that exert the most significant influence on the overall microbiome-metabolite interaction. This hypothesis is grounded in recent studies, such as Liu et al. (2022), which explore the relationship between microbiome composition and metabolite production, demonstrating that specific microbiome species substantially affect the types and concentrations of metabolites within a host organism. Consequently, it is essential to impose sparsity on the \mathbf{B} -matrix in a structured manner. It is also important to ensure that the proposed model not only achieves overall sparsity but also facilitates the identification of critical predictors, enabling a biologically interpretable understanding of the microbiome-metabolite relationship. A conceptual diagram of ‘master predictors’, which are subsequently identified using B-MASTER, is presented in Figure 1.

2.2 Prior Formulation

Extensive research on variable selection has demonstrated that, in scenarios with a large number of covariates, the relationships between predictors and responses are frequently governed by a small subset of influential predictors (Qian et al. 2020). Prominent penalized regression methods, such as LASSO (Tibshirani 1996) and SCAD (Fan & Li 2001), are specifically designed to identify these sparse structures, even under conditions of multicollinearity or strong correlations among predictors. The application of an l_1 -penalty to the coefficients of \mathbf{B} encourages overall sparsity by shrinking many coefficients to zero. Fur-

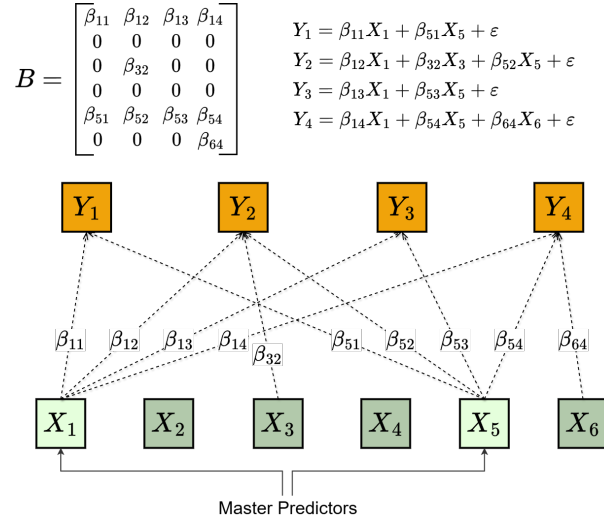


Figure 1: Conceptual diagram of ‘master predictors’, subsequently identified using B-MASTER.

thermore, to discern predictors that exert a dominant influence across multiple response components, an additional l_2 -norm can be imposed on the individual coefficient vectors associated with each predictor (Peng et al. 2010). This hybrid penalization approach ensures the selection of a parsimonious model while simultaneously introducing a shrinkage effect on the coefficients linked to predictors with less significant impacts. Adhering to our intended set of penalizing constraints, following Kyung et al. (2010) the conditional prior of \mathbf{B} is given by

$$\pi(\mathbf{B}|\sigma_1^2, \dots, \sigma_Q^2) \propto \exp \left[-\lambda_1 \sum_{p=1}^P \sum_{q=1}^Q \frac{|\beta_{pq}|}{2\sigma_q^2} - \lambda_2 \sum_{p=1}^P \left(\sum_{q=1}^Q \frac{\beta_{pq}^2}{2\sigma_q^2} \right)^{1/2} \right]. \quad (2)$$

Upon closer examination, it becomes evident that λ_1 governs the overall shrinkage of all coefficients, while λ_2 introduces a penalty on the l_2 -norm of the coefficients corresponding to the individual components of X . To extend the framework in equation (2), we incorporate prior knowledge regarding the susceptibility of sparsity in certain elements of \mathbf{B} . Let $\mathbf{C} = (c_{pq})$ be a pre-specified $P \times Q$ binary matrix, such that, the values of c_{pq} corresponding to the set of coefficients in \mathbf{B} , which are known to have non-zero effect on Y , are set to 0, and the remaining elements are set to 1. Based on this prior information, the updated conditional prior for \mathbf{B} is as follows:

$$\pi(\mathbf{B}|\sigma_1^2, \dots, \sigma_Q^2) \propto \exp \left[-\lambda_1 \sum_{p=1}^P \sum_{q=1}^Q \frac{|c_{pq}\beta_{pq}|}{2\sigma_q^2} - \lambda_2 \sum_{p=1}^P \left\{ \sum_{q=1}^Q \frac{(c_{pq}\beta_{pq})^2}{2\sigma_q^2} \right\}^{1/2} \right]. \quad (3)$$

It is important to highlight several caveats associated with the straightforward application of analogous frequentist approaches for optimizing the coefficient matrix \mathbf{B} within a similar penalized likelihood framework, as discussed in (Peng et al. 2010) (hereafter referred to as ‘remMap’). First, remMap employs the “active-shooting” algorithm (Friedman et al. n.d., Peng et al. 2009) to optimize \mathbf{B} for a given λ_1 , which operates with a computational complexity of $O(NPQ)$. Consequently, as the sample size increases, the computational burden becomes substantially heavier, a drawback not encountered in the proposed Gibbs sampler algorithm which exhibits nearly constant computation time even as the sample size grows. This efficiency arises from the fact that only a small fraction of the overall computation time is dedicated to dataset-related operations. Additionally, the dataset-dependent computations in our method primarily involve matrix multiplications, which are efficiently handled by the multi-threading capabilities of MATLAB. As matrix size increases (due to N), higher levels of multi-threading are activated, leading to only a minor increase in computation time as N grows (MathWorks 2024). Thus, for fixed values of P and Q , the computation time of the Gibbs sampler algorithm remains largely invariant with respect to sample size. In Figure 2 (see Section 3.2 for data generation mechanism), we illustrate how the computation time for remMap is strongly dependent on the sample size, while B-MASTER exhibits near invariance with respect to sample size.

Second, the process of selecting an optimal λ_1 via cross-validation further intensifies the computational demands. If uncertainty quantification is required, bootstrapping procedures may lead to prohibitively long computation times. A detailed investigation of the performance limitations of remMap in high-dimensional settings is provided in the subsequent simulation study section. These challenges can be mitigated by adopting a Bayesian framework, where model estimation is conducted once, yielding both optimal coefficients and their associated uncertainty measures.

Lastly, the computational time per iteration of the proposed Gibbs sampler remains independent of the dataset characteristics, provided the dimensions P and Q are fixed. In contrast, the “active-shooting” algorithm in remMap demonstrates a high degree of data

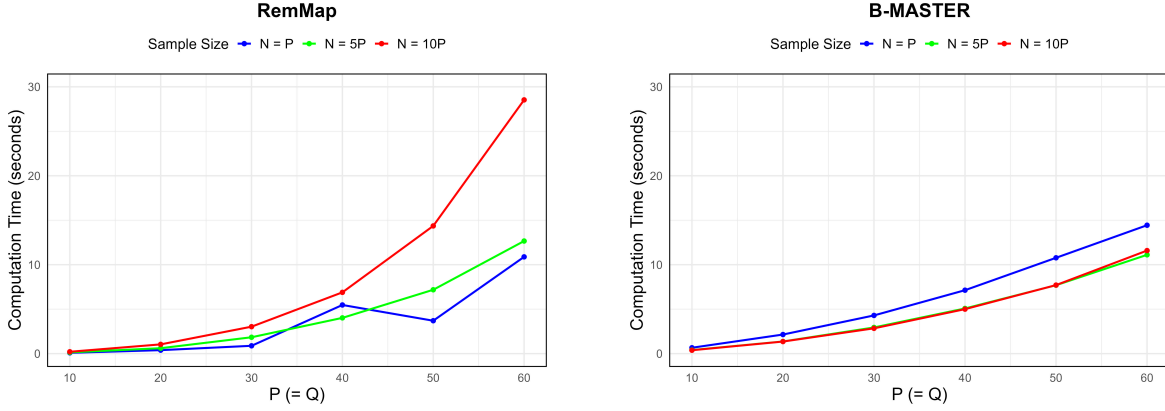


Figure 2: The required computation times for $P = Q = 10, 20, 30, 40, 50, 60$ are shown for remMap (left) and B-MASTER, with $N = P, 5P, 10P$. The data generation mechanism is same as the one used in the simulation study presented in Section 3.2.

dependence, with convergence time substantially influenced by specific dataset properties. Specifically, remMap exhibits considerable variability in convergence times for datasets of identical dimensionality. For example, as illustrated in Figure 2 (left), with $P = Q = 40$, the computation time for $N = 40$ exceeded that for $N = 200$ and was also longer than for the case where $P, Q = 50, N = 50$. Whereas the computation time for B-MASTER is observed to increase in a more predictable, robust fashion as P grows. It is observed that B-MASTER takes slightly more time for $N = P$ scenarios compared to $N = 5P$ and $N = 10P$ scenarios. We speculate that it results from the well-known fact that higher dimensional matrix algebraic operations can potentially trigger higher amount of multi-threading activation in MATLAB (MathWorks 2024).

Now we formalize the explicit prior structure picking up from (3). Upon close inspection, prior distribution described in (3) indicates that between predictors they are independent, however within a predictor type there is dependency across all coefficients corresponding to the Q response components. Let us denote the coefficient vector for the p -th predictor by $\boldsymbol{\beta}^{(p)} = (\beta_{p1}, \dots, \beta_{pQ})$. Now (2) can be re-structured as

$$\pi(\mathbf{B} | \sigma_1^2, \dots, \sigma_Q^2) = \prod_{p=1}^P \pi(\boldsymbol{\beta}^{(p)} | \sigma_1^2, \dots, \sigma_Q^2), \text{ where,}$$

$$\pi(\boldsymbol{\beta}^{(p)} | \sigma_1^2, \dots, \sigma_Q^2) \propto \exp \left[-\lambda_1 \sum_{q=1}^Q \frac{|c_{pq}\beta_{pq}|}{2\sigma_q^2} - \lambda_2 \left\{ \sum_{q=1}^Q \frac{(c_{pq}\beta_{pq})^2}{2\sigma_q^2} \right\}^{1/2} \right]. \quad (4)$$

We introduce latent parameters $\mathbf{T}^2 = (\boldsymbol{\tau}_1^2, \dots, \boldsymbol{\tau}_P^2)^T = (\tau_{pq}^2)_{P \times Q}$ and $\mathbf{G}^2 = (\boldsymbol{\gamma}_p^2)_{P \times 1}$.

This formulation enables us to express the expression in (4) within a hierarchical structure for $c_{pq} = 1$ (Xu & Ghosh 2015), as follows:

$$\boldsymbol{\beta}^{(p)} | \boldsymbol{\tau}_p^2, \gamma_p^2, \sigma_1^2, \dots, \sigma_Q^2 \sim N_Q(\mathbf{0}, \mathbf{V}_p), \quad (5)$$

$$\pi(\boldsymbol{\tau}_p^2, \gamma_p^2) \propto C_p^*(\lambda_1^2, \lambda_2^2) \prod_{q=1}^Q \left[(\tau_{pq}^2)^{-1/2} \left(\frac{1}{\tau_{pq}^2} + \frac{1}{\gamma_p^2} \right)^{-1/2} \right] (\gamma_p^2)^{-1/2} \exp \left\{ -\frac{\lambda_1^2}{2} \sum_{q=1}^Q \tau_{pq}^2 - \frac{\lambda_2^2}{2} \gamma_p^2 \right\} \quad (6)$$

where,

$$\mathbf{V}_p = \text{diag} \left\{ \sigma_q^2 \left(\frac{1}{\tau_{pq}^2} + \frac{1}{\gamma_p^2} \right)^{-1} \right\} \text{ for } q = 1, \dots, Q,$$

and $C_p^*(\lambda_1^2, \lambda_2^2)$ is a normalizing term involving both penalty terms. The propriety of the prior distribution introduced in (6) is established in the supplementary material. We put an non-informative prior on σ_q^2 as follows:

$$\pi(\sigma_q^2) \propto \frac{1}{\sigma_q^2}, \text{ for } q = 1, \dots, Q. \quad (7)$$

Hereafter, combining the likelihood from the model (1) along with the aforementioned prior setup, we obtain the joint posterior distribution:

$$\begin{aligned} \pi(\mathbf{B}, \mathbf{T}^2, \mathbf{G}^2, \boldsymbol{\sigma}^2, | \mathbf{X}, \mathbf{Y}) &\propto \prod_{q=1}^Q \left[(\sigma_q^2)^{-\frac{(N+\sum_p c_{pq})}{2}-1} \exp \left\{ -\frac{(\mathbf{y}_q - \mathbf{X}\boldsymbol{\beta}_q)'(\mathbf{y}_q - \mathbf{X}\boldsymbol{\beta}_q) + \boldsymbol{\beta}_q' D_{\tau_q} \boldsymbol{\beta}_q}{2\sigma_q^2} \right\} \right] \\ &\prod_{p=1}^P \left[C_p^*(\lambda_1^2, \lambda_2^2) \prod_{q=1: c_{pq}=1}^Q \left\{ (\tau_{pq}^2)^{-1/2} \left(\frac{1}{\tau_{pq}^2} + \frac{1}{\gamma_p^2} \right)^{-1/2} \right\} (\gamma_p^2)^{-1/2} \right] \\ &\exp \left\{ -\frac{\lambda_1^2}{2} \sum_{q=1}^Q \tau_{pq}^2 - \frac{\lambda_2^2}{2} \gamma_p^2 \right\} \end{aligned} \quad (8)$$

where $\mathbf{y}_q = (y_q^1, y_q^2, \dots, y_q^N)$ denotes the q -th component (column) of the response matrix \mathbf{Y} ($N \times Q$ matrix of response); $\mathbf{x}^i = (x_1^i, x_2^i, \dots, x_P^i)$ denotes the i -th row of the covariate matrix \mathbf{X} ($N \times P$ matrix of covariates); and D_{τ_q} is a $P \times P$ diagonal matrix such that $D_{\tau_q}(p, p) = \frac{1}{\tau_{pq}^2} + \frac{1}{\gamma_p^2}$ for $p = 1, \dots, P$, and remains relevant only when $c_{pq} = 1$.

2.3 Gibbs Sampling

From the joint posterior distribution (8), we derive a Gibbs sampling algorithm to generate posterior samples of $\mathbf{B} = (\beta_{pq})_{P \times Q}$, $\mathbf{T}^2 = (\tau_1^2, \dots, \tau_P^2)^T = (\tau_{pq}^2)_{P \times Q}$, $\mathbf{G}^2 = (\gamma_p^2)_{P \times 1}$, and $\boldsymbol{\sigma}^2 = (\sigma_1^2, \sigma_2^2, \dots, \sigma_Q^2)$ from their full conditional posteriors as follows,

- Sample $\boldsymbol{\beta}_q = (\beta_{1q}, \dots, \beta_{Pq})^T$ for $q = 1, \dots, Q$, from

$$\boldsymbol{\beta}_q | \mathbf{T}^2, \mathbf{G}^2, \sigma_q^2 \sim N_p \left((\mathbf{X}'\mathbf{X} + D_{\tau_q})^{-1} \mathbf{X}'\mathbf{y}_q, \sigma_q^2 (\mathbf{X}'\mathbf{X} + D_{\tau_q})^{-1} \right).$$

- Sample τ_{pq}^2 , only if $c_{pq} = 1$, for $p = 1, \dots, P; q = 1, \dots, Q$, such that $\tau_{pq}^2 = \frac{1}{\delta_{pq}^{(1)}}$, where

$$\delta_{pq}^{(1)} | \beta_{pq}, \sigma_q^2, \lambda_1^2 \sim \text{Inv-Gaussian} \left(\sqrt{\frac{\lambda_1^2 \sigma_q^2}{\beta_{pq}^2}}, \lambda_1^2 \right).$$

- Sample γ_p^2 for $p = 1, \dots, P; q = 1, \dots, Q$, such that $\gamma_p^2 = \frac{1}{\delta_p^{(2)}}$, where

$$\delta_p^{(2)} | \mathbf{B}, \boldsymbol{\sigma}^2, \lambda_2^2 \sim \text{Inv-Gaussian} \left(\sqrt{\frac{\lambda_2^2}{\sum_{q=1}^Q (\beta_{pq}^2 / \sigma_q^2)}}, \lambda_2^2 \right).$$

- Sample σ_q^2 for $q = 1, \dots, Q$, from

$$\sigma_q^2 | \boldsymbol{\beta}_q, \mathbf{T}^2, \mathbf{G}^2 \sim \text{Inv-Gamma}(a_q, b_q)$$

$$\text{where } a_q = \frac{N + \sum_p c_{pq}}{2}, b_q = \frac{(\mathbf{y}_q - \mathbf{X}\boldsymbol{\beta}_q)'(\mathbf{y}_q - \mathbf{X}\boldsymbol{\beta}_q) + \boldsymbol{\beta}_q' D_{\tau_q} \boldsymbol{\beta}_q}{2}.$$

Note that the tuning parameters in (8) are incorporated as fixed values. Thus, this proposed sampling scheme can be used to perform posterior inference of B-MASTER parameters for given fixed values of the tuning parameters λ_1 and λ_2 . We further delve into putting appropriate hyper-prior on the the prior parameters in the following sub-section.

2.4 Prior on Tuning Parameters and Gibbs Sampling

The Gibbs sampling scheme outlined in the previous subsection is conceptually analogous to the sparse model estimation process within the frequentist framework. In the frequentist setting, for fixed values of the tuning parameters, the model is fitted, and optimal tuning

parameter values are subsequently selected through methods such as cross-validation or approaches based on Stein’s unbiased risk estimate (Tibshirani 1996). In contrast, the Bayesian framework circumvents this extended cross-validation process by assigning suitable hyper-priors to λ_1 and λ_2 (Park & Casella 2008, Kyung et al. 2010, Roy & Chakraborty 2017). This facilitates a fast and efficient mechanism for sampling λ_1 and λ_2 simultaneously with other model parameters. Following the recommendations of Kyung et al. (2010) and Xu & Ghosh (2015), we assign the following joint prior distribution to λ_1^2 and λ_2^2 :

$$\pi(\lambda_1^2, \lambda_2^2) \propto C(\lambda_1^2, \lambda_2^2)(\lambda_1^2)^{a_1} \exp(-b_1\lambda_1^2)(\lambda_2^2)^{a_2} \exp(-b_2\lambda_2^2), \quad (9)$$

where $C(\lambda_1^2, \lambda_2^2) = \left(\prod_{p=1}^P C_p^*(\lambda_1^2, \lambda_2^2)\right)^{-1}$ and a_1, b_1, a_2, b_2 are some positive constants.

Such a prior structure is well-studied in the context of Bayesian group lasso and sparse graphical models (Xu & Ghosh 2015, Das et al. 2020). Following their recommendation, to impose a stronger penalization structure as the number of parameters in the coefficient matrix requiring penalization (i.e., $\sum_{p,q} c_{pq}$) increases, hyper-prior parameter values are chosen as $a_1 = \sum_{p,q} c_{pq} + r_1$ and $a_2 = \frac{1}{2} \sum_{p,q} c_{pq} + r_2$, where r_1 and r_2 are positive constants. This prior structure is found to perform well across a broad range of P and Q values, maintaining excellent control over the true positive rate (TPR) and false positive rate (FPR), without issues in both low and high-dimensional scenarios, as detailed in Section 3. The propriety of the prior introduced in (9) is discussed in detail in the supplementary material. The conditional posterior distributions of the tuning parameters are given as follows:

$$\lambda_1^2 | \mathbf{T}^2 \sim \text{Gamma}\left(\sum_{p,q} c_{pq} + a_1, \frac{1}{2} \sum_{p,q:c_{pq}=1} \tau_{pq}^2 + b_1\right), \quad (10)$$

$$\lambda_2^2 | \mathbf{G}^2 \sim \text{Gamma}\left(\frac{1}{2} \sum_{p,q} c_{pq} + a_2, \frac{1}{2} \sum_{p=1}^P \gamma_p^2 + b_2\right). \quad (11)$$

Note that the full conditional posterior distributions of λ_1^2 and λ_2^2 do not involve any computation of $C(\lambda_1^2, \lambda_2^2)$ resulting in substantial improvement in computational efficiency. By integrating the sampling steps for λ_1^2 and λ_2^2 outlined above with the Gibbs sampling procedure detailed in Section 2.3, the complete Gibbs sampling framework for B-MASTER is established.

3 Simulation Studies

In this section, we consider two simulation studies. In the first study, we compare the performance of the proposed B-MASTER method with a few existing methods using a synthetic dataset generated mimicking the real dataset. This simulation study allows us to benchmark B-MASTER against other existing methods while keeping X unchanged, thereby retaining the original covariance structure of the dataset. This setup enables us to investigate relative performances in a more practical and relevant context, aligned with our ultimate goal of analyzing the real dataset. In the second study, we focus primarily on evaluating the computational performance of B-MASTER in a different set up as the dimensions of X and Y increase.

3.1 Real-data Based Simulation Study

The real dataset (Yachida et al. 2019), described and analyzed later in this paper, consists of $P = 287$ microbiome features and $Q = 249$ metabolite features from $N = 220$ subjects. Using B-MASTER, the optimal B' is first estimated and then considered the true coefficient matrix for the simulation study. Then, we generate

$$Y_q^i = X^i B'_q + \epsilon_{iq}$$

for $i = 1, \dots, N$, where $B'_q = (\beta'_{pq})_{p=1}^P$ denotes the q -th column of B' and $\epsilon_{iq} \sim N(0, \sigma^2)$; we take $\sigma = 1$. Ten sets of synthetic Y are generated, followed by the performance evaluation of B-MASTER and other methods using the actual X (as in the original dataset) and B' .

B-MASTER is implemented in MATLAB. The values of the model parameters are as follows: $r_1 = 1, r_2 = 1, \delta_1 = 0.1, \delta_2 = 0.1$ and $c_{pq} = 1$ for all $p = 1, \dots, P$ and $q = 1, \dots, Q$. B-MASTER is run for 1,000 iterations discarding the first 100 posterior samples as burn-in. It is observed that the results obtained using B-MASTER under the aforementioned setup are not noticeably different from those obtained after 100 iterations, discarding the first 10 iterations as burn-in. However, for the comparative study, the analysis results are reported under the first setup (i.e., 1,000 iterations with 100 burn-in).

To identify the non-significant coefficients, we construct a two-sided symmetric 90% posterior credible interval for each β_{pq} based on the posterior samples. Coefficients β_{pq} s

whose posterior credible intervals contain 0 are discarded as non-significant. To calculate the area under the Receiver Operating Characteristic (ROC) curve (AUC), Bayesian p-values corresponding to each β_{pq} are computed as follows. Suppose $\{\beta_{pq}^{(1)}, \dots, \beta_{pq}^{(M)}\}$ denote the posterior sample values of coefficient β_{pq} . Let \hat{p}^+ denote the the proportion of β_{pq} samples which are > 0 ; and let \hat{p}^- denote the the proportion of β_{pq} samples which are ≤ 0 . Then

$$\text{Bayesian p-value} = 2 * \min(\hat{p}^+, \hat{p}^-).$$

We take an equidistant grid of cut-off points of length 501 over the interval $[0, 0.5]$. For each cut-off point, we calculate the true positive rate (TPR) and false positive rate (FPR) based on Bayesian p-values. Additionally, we compute AUC20 (i.e., $\text{AUC20} = 5 \times \text{Area}$ under the ROC curve up to 20% FPR) and Mathew’s Correlation Coefficient (MCC) (Chicco & Jurman 2020), which is given by

$$\text{MCC} = \frac{TP \cdot TN - FP \cdot FN}{\sqrt{(TP + FP)(TP + FN)(TN + FP)(TN + FN)}},$$

where TP, TN, FP, FN denote true positives, true negatives, false positives and false negatives, respectively.

For the comparative study, we consider a few existing methods, namely Regularized Multivariate regression for identifying master predictors (Peng et al. 2010), univariate and multivariate Spike-and-Slab LASSO (Rockova & George 2018, Deshpande et al. 2019); hereafter referred to as remMap, SSLASSO and mSSL, respectively. SSLASSO and mSSL employ spike-and-slab LASSO in the frequentist framework, which, unlike remMap or B-MASTER, does not impose an additional L2 penalty to discourage non-essential regressors. RemMap is implemented using the R package `remMap` (Peng et al. 2010). It should be noted that the `remMap` package provides two ways to estimate the coefficient matrix. The first method involves using the function `remMap.CV` to perform cross-validation over a predefined grid of tuning parameter values. This is followed by fitting the model using the function `remMap` with the optimal tuning parameters determined in the first step. The alternative function, `remMap.BIC` selects the best model using the Bayesian Information Criterion (BIC, Schwarz (1978)) over a grid of given values for the tuning parameters. The authors noted that the second method is computationally more feasible. They also pointed out that this alternative BIC-based option tends to select models that are too small when the

Methods	TPR	FPR	MCC	AUC	AUC20	Sparsity (True = 0.76)
B-MASTER	0.84 (0.0012)	0.01 (0.0003)	0.87 (0.0001)	0.98 (0.0004)	0.94 (0.0014)	0.79 (0.0003)
SSLASSO	0.23 (0.0008)	0.01 (0.0004)	0.41 (0.0013)	0.89 (0.0004)	0.54 (0.0007)	0.94 (0.0002)
mSSL-dcpe	0.14 (0.0018)	0.00 (0.0001)	0.31 (0.0024)	0.76 (0.0006)	0.44 (0.0013)	0.96 (0.0005)
remMap-bic	0.00 (0.0001)	0.00 (0.0000)	0.02 (0.0008)	0.58 (0.0015)	0.23 (0.0009)	1.00 (0.0000)

Table 1: A comparative study of B-MASTER, SSLASSO, mSSL, and remMap based on the true positive rate (TPR), false positive rate (FPR), Matthew’s Correlation Coefficient (MCC), Area under the ROC curve (AUC), and AUC20 from 10 simulation experiments is presented. Mean measure values are provided, with standard errors in parentheses.

actual design matrix is far from orthogonal. For both `remMap` and `remMap.BIC`, we use a grid of λ_1 values that are exponential of an equidistant grid of length 11, spanning over the range from 0 and $\log(1000)$. λ_2 values are taken to be an equidistant grid of length 11, spanning over the range from 0 and 1000. We opt for 5-fold cross-validation. SSLASSO and mSSL are implemented using R packages `SSLASSO` (Rockova & George 2018) and `mSSL` (Deshpande et al. 2019), respectively. SSLASSO is fit using the `SSLASSO` function within the package of the same name. The R package `mSSL` offers to model-fitting options, namely `mSSL_dpe` and `mSSL_dcpe`, respectively. `mSSL_dpe` performs the Expectation-Conditional Maximization (ECM) algorithm, which targets the MAP estimates of the coefficient matrix. `mSSL_dcpe` is proposed as a faster approximate alternative of `mSSL_dpe`. We opt for the default option to select the grid of tuning parameter values. Note that, for all the above-mentioned methods, the results corresponding to the respective grids are later used to calculate AUC and AUC20.

All simulation experiments are performed on a desktop running the Windows 10 Enterprise operating system desktop with 32 GB RAM and the following processor characteristics: 12th Gen Intel(R) Core(TM) i7-12700, 2100 Mhz, 12 Cores(s), 20 Logical Processor(s). We observe that `mSSL_dpe` and `remMap.CV` did not terminate or produce results within 48 hours, possibly due to the high number of parameters considered ($P*Q = 249 \times 287 = 71463$) in the simulation settings. We report only the results corresponding to the methods `mSSL` and `remMap`, using the functions `mSSL_dcpe` (from the R package `mSSL`) and `remMap.BIC` (from the R package `remMap`). The calculated TPR, FPR, MCC, AUC, AUC20, and sparsity proportion of the estimated coefficient matrices under different methods are provided in Table 1. The standard errors for all considered measures are noted in parentheses. We observe that B-MASTER outperforms SSLASSO, mSSL, and RemMap by a large margin. It is noted that, except for B-MASTER, the other methods overly shrink the coefficients,

resulting in a very low TPR. In terms of AUC, SSLASSO performed the best among the other methods. We would like to point out to the readers that, since the original functions for mSSL and RemMap did not converge within 48 hours, we were only able to use their approximate, faster alternative versions, which are susceptible to the over-shrinking issue, as mentioned by the corresponding authors.

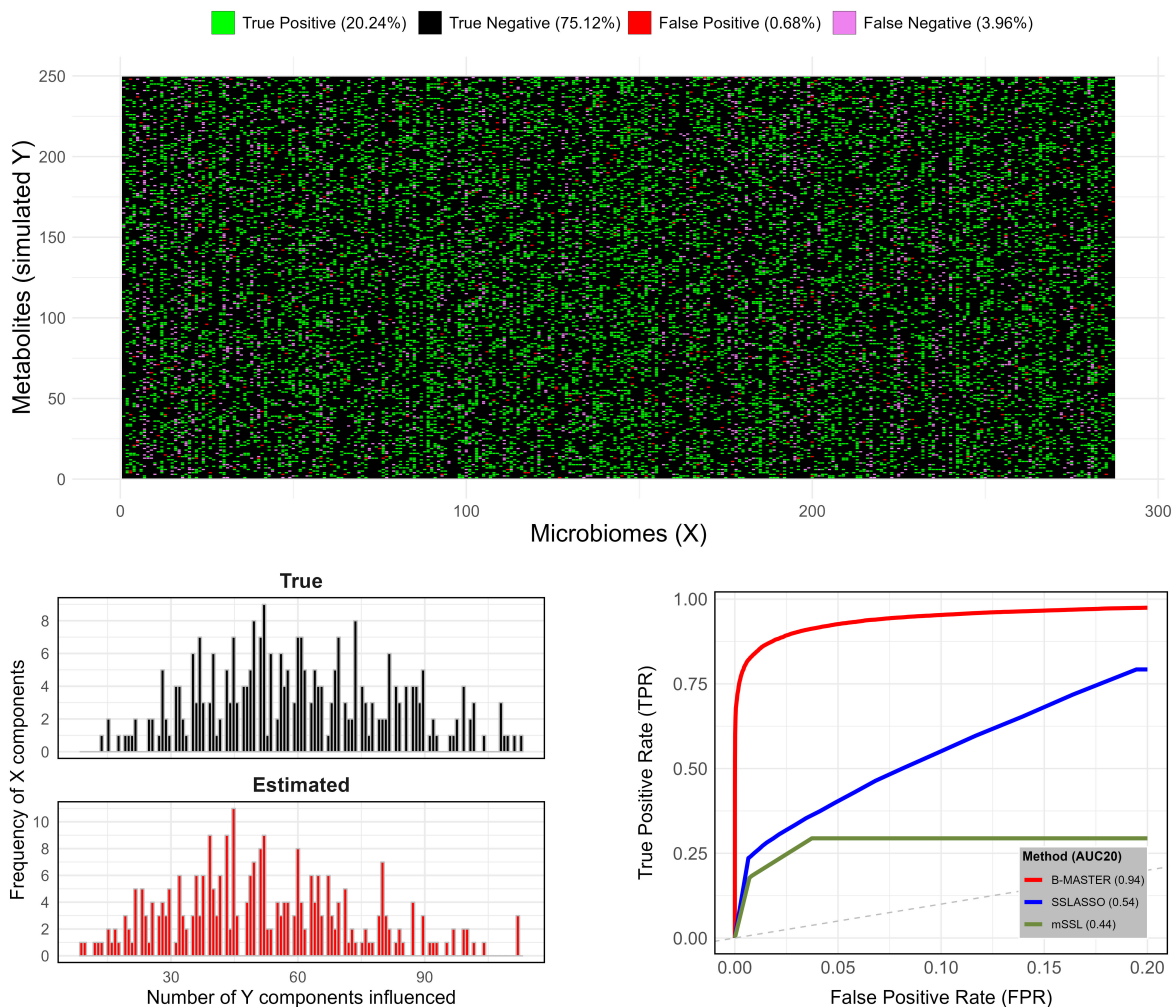


Figure 3: *Up*: Signal detection performance of B-MASTER is evaluated based on Simulation Study 1. True and B-MASTER estimated coefficient signals are depicted, divided into categories: true positives (TP), true negatives (TN), false positives (FP), and false negatives (FN). *Bottom-left*: True and B-MASTER estimated numbers of Y components influenced by X components are depicted. *Bottom-right*: The AUC curve is plotted up to a false positive rate of 20% for the B-MASTER, SSLASSO, and mSSL methods. AUC20 values are provided in parentheses within the legend.

In Figure 3 (*up*), the true and B-MASTER estimated coefficient signals are depicted, divided into four categories: TP, TN, FP, and FN. The number of Y components influenced

by X components under both true and B-MASTER estimated scenarios is shown as a histogram in Figure 3 (*bottom-left*). It appears that B-MASTER is slightly conservative in selecting variables, which creates a slight leftward shift in the histograms under the B-MASTER estimated scenario. Figure 3 (*bottom-right*) shows that the AUC curve of B-MASTER dominates over SSLASSO and mSSL across the FPR range from 0% to 20%, by a large margin. We chose to display the AUC curve up to the 20% FPR zone because the grid points of FPR and TPR obtained from the SSLASSO and mSSL model fittings (with grids taken as default options) were very sparse for FPR values greater than 20%. We refrain from plotting the AUC curve for remMap, as Table 1 already indicates its under-performance in the considered experiment.

3.2 Evaluation of B-MASTER in Higher Dimensions

To evaluate the performance and required computation times in higher-dimensional settings for B-MASTER, we conduct another simulation study. We generate N realizations of X from $MVN(\mathbf{0}, \Sigma)$, where $\Sigma = (\rho_{i,j})_{P \times P}$ with $\rho_{i,j} = \rho^{|i-j|}$. We then generate \mathbf{B}_0 (a matrix of dimension $P \times Q$), where each element of \mathbf{B}_0 is sampled from $U([-5, -1] \cup [1, 5])$. Hereafter, we generate an indicator matrix to impose sparse structure over the coefficient matrix adhering to the following presumptions:

- 20% of the X components influence all Y components.
- Another 20% of the X components influence 100s% of the Y components selected at random, where $s \sim U(.4, .6)$.
- The remaining 60% X components are assumed to have no effect on Y .

We construct an indicator matrix I_0 of dimension $P \times Q$, where 1s and 0s are assigned based on the aforementioned assumptions. Finally, we compute $\mathbf{B} = \mathbf{B}_0 \circ I_0$, where \circ denotes element-wise product. Then, we generate

$$Y_q^i = X^i B_q + \epsilon_{iq}$$

for $i = 1, \dots, N$, where $B_q = (\beta_{pq})_{p=1}^P$ denotes the q -th column of \mathbf{B} and $\epsilon_{iq} \sim N(0, \sigma^2)$; we take $\sigma = 0.1$. For all considered scenarios, we set $P = Q = N$ inspired by the fact that

in the real-dataset, the values of P, Q, N are similar ($P = 287, Q = 249, N = 220$). The performance of B-MASTER is evaluated for $P = 20, 50, 100, 200, 500, 100, 2000$. All these sub-scenarios considered taking ρ to be 0 (independent components) and 0.5 (highly correlated components), separately. The simulation results are provided in Table 2. For each case, along with TPR, FPR, MCC, AUC, AUC20, estimated sparsity, and true sparsity (in parentheses), we also report the computation times. Although the results are based on 100 iterations with 20 burn-in, the projected time to complete 1000 iterations is also provided. Since each iteration takes a similar amount of time for a given dimensional setting, the projected time to complete 1000 iterations is approximately 10 times the time spent performing 100 iterations. Note that, for the experiments considered, we did not observe any further noticeable improvement when using 1000 iterations instead of 100. It was observed that for both cases, across all considered dimensions, B-MASTER performed well, yielding near-perfect TPR, FPR, AUC, MCC, and AUC20. The estimated sparsity was also very close to the true sparsity, showing a slight trend toward being conservative, which resulted in the estimated \mathbf{B} being marginally sparser than the true model. The B-MASTER results for the independent X scenario are slightly better than those for the correlated case. Furthermore, as the dimension of the parameter space increases, the computation time increases linearly, making it highly scalable for higher-dimensional models. This scalability enables us to evaluate B-MASTER performance in a model with up to 4 million coefficients within a reasonable amount of time. In Figure 4, we demonstrate the log-log plot (with base 10) of the number of parameters vs. computation time (in minutes) for B-MASTER in the $\rho = 0.5$ scenario, revealing a linear dependence relationship. The approximate value of the slope is noted to be 1.06. The plot for the $\rho = 0$ scenario is nearly identical, and therefore, we refrain from plotting it.

4 Identification of Key Genera in Microbiome-Metabolite Dynamics Associated with Colorectal Cancer

Background: The gut microbiome can significantly influence the response to cancer therapies, including immunotherapies, largely through its impact on the metabolome (Malczewski et al. 2020). Metabolites produced by the gut microbiota, such as short-chain fatty

ρ	P, Q, N	TPR	FPR	MCC	AUC	AUC20	Sparsity (true sparsity)	Number of parameters	Number of parameter folds	Comp. time for 100 iters. (in mins)	Comp.time folds	Comp. time for 1000 iters. (projected, in mins)
$\rho = 0$	20	0.974	0.000	0.982	0.999	0.999	0.715 (0.708)	400	1x	0.04	1x	0.37
	50	0.991	0.000	0.993	1.000	1.000	0.708 (0.705)	2500	6.25x	0.19	5.24x	1.94
	100	0.978	0.012	0.964	0.997	0.986	0.699 (0.700)	10000	25x	0.74	19.97x	7.39
	200	0.972	0.026	0.937	0.995	0.980	0.692 (0.702)	40000	100x	4.68	126.38x	46.76
	500	0.996	0.029	0.951	0.998	0.990	0.681 (0.699)	250000	625x	26.68	721.03x	266.78
	1000	0.998	0.006	0.989	0.999	0.999	0.697 (0.700)	1000000	2500x	108.34	2928.19x	1083.43
	2000	0.998	0.000	0.998	1.000	1.000	0.702 (0.701)	4000000	10000x	603.65	16314.87x	6036.50
	20	0.966	0.000	0.976	1.000	1.000	0.718 (0.708)	400	1x	0.04	1x	0.36
$\rho = 0.5$	50	0.999	0.002	0.996	1.000	1.000	0.704 (0.705)	2500	6.25x	0.19	5.14x	1.85
	100	0.982	0.025	0.947	0.994	0.970	0.689 (0.700)	10000	25x	0.71	19.64x	7.07
	200	0.963	0.033	0.921	0.992	0.969	0.690 (0.702)	40000	100x	4.78	132.72x	47.78
	500	0.990	0.021	0.959	0.998	0.991	0.688 (0.699)	250000	625x	27.84	773.39x	278.42
	1000	0.984	0.001	0.988	1.000	1.000	0.705 (0.700)	1000000	2500x	119.65	3323.53x	1196.47
	2000	0.947	0.000	0.963	1.000	0.999	0.717 (0.701)	4000000	10000x	644.97	17915.75x	6449.67

Table 2: Performance evaluation of B-MASTER: The values of P ($P = Q = N$), TPR, FPR, MCC, AUC, AUC20, sparsity (with true sparsity in parentheses), the number of parameters, relative folds of the number of parameters, computation time for 100 iterations (in minutes), relative folds of computation times, and the projected computation time for 1000 iterations (in minutes) are provided taking $P = Q = N = 20, 50, 100, 200, 500, 1000, 2000$ under scenarios $\rho = 0, 0.5$.

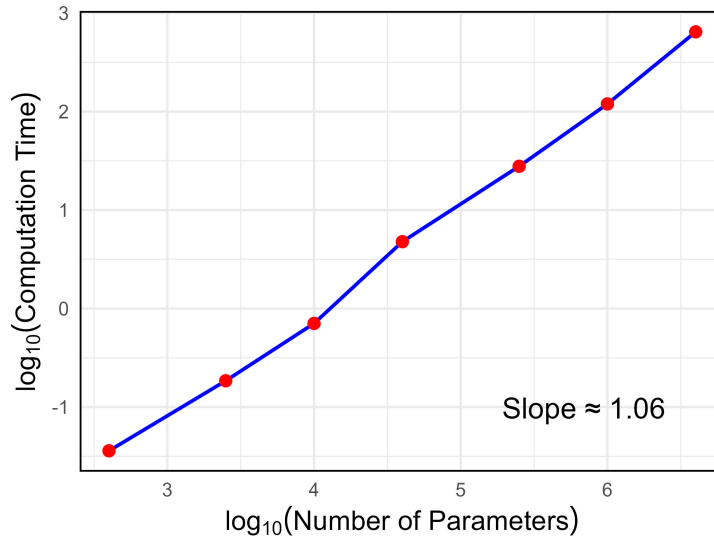


Figure 4: The plot shows $\log_{10}(\text{Number of Parameters})$ versus $\log_{10}(\text{Computation Time})$ for B-MASTER applied across scenarios with $P = Q = N = (20, 50, 100, 200, 500, 1000, 2000)$ and $\rho = 0.5$. Computation time is measured in minutes.

acids (SCFAs), can modulate the immune system, including promoting T cell differentiation and regulating tumor-associated immunity. These microbial metabolites may enhance or inhibit the effectiveness of therapies like immune checkpoint inhibitors (ICIs). For example, certain microbial metabolites have been linked to improved immune responses and tumor control in patients undergoing cancer treatments (Lu et al. 2022). Therefore, it is crucial to understand the inherent mechanisms by which metabolites are influenced by the gut microbiota. If our objective were to identify the specific set of genera impacting a particular metabolite, fitting LASSO (Tibshirani 1996) could offer a valuable overview by selecting relevant predictors. However, given that our primary goal is to understand which genera within the microbiome play a pivotal role in shaping the overall metabolome, aligning with our research objectives, it is more appropriate to identify the essential regressors within the microbiome that exert influence over a broad spectrum of metabolites. This approach ensures a comprehensive understanding of the microbiota-metabolome interaction, emphasizing the systemic contributions of key microbial taxa.

Data source and pre-processing: Microbiome and metabolite profiles for colorectal cancer cases were obtained from 220 subjects based on the study by Yachida et al. (2019). The processed data were sourced from The Curated Gut Microbiome-Metabolome Data Resource (Muller et al. 2022). To reduce the prevalence of highly zero-inflated features,

microbiome data were summarized at the genus level and filtered to include only genera present in at least 20% of subjects, with an average abundance of at least 0.01%. A centered-log-ratio transformation was applied to the microbiome abundances prior to analysis. Metabolites were filtered to those present in at least 20% of samples, and one-half of the minimum value was added to zero values before log transformation. This resulted in a set of 287 genera and 249 metabolites included in the regression model. To visually illustrate the dataset, score plots from Principal Component Analysis (PCA) of microbiome and metabolite components (after transformation) are depicted in Figure 5.

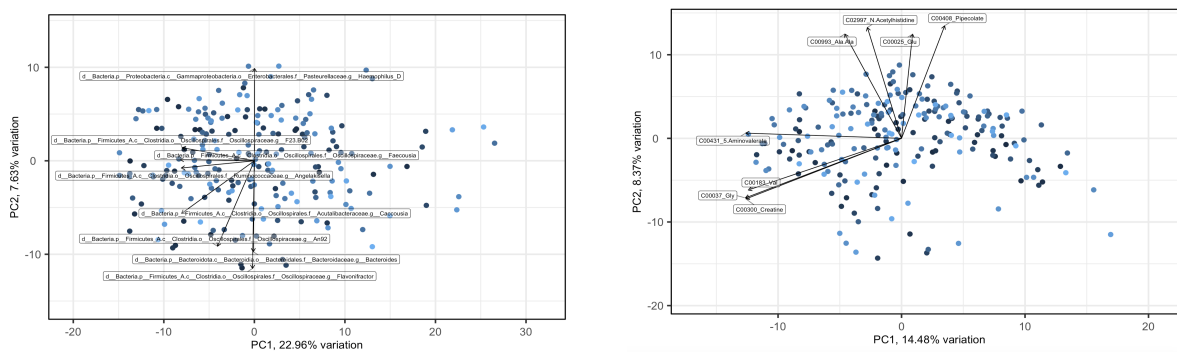


Figure 5: Score plots from Principal Component Analysis (PCA) illustrating the distribution of $P = 287$ microbial genera (left) and $Q = 249$ metabolites (right) based on fecal samples collected from $N = 220$ patients.

Overall analysis and findings: In order to identify the key microbiome components influencing metabolites, B-MASTER is fitted with hyper-parameter values consistent with those used in the simulation study. Inference is performed based on posterior samples generated over 2000 iterations, with the first 100 iterations discarded as burn-in. Using B-MASTER, we identify the top 50 microbiome taxa that influence the greatest number of metabolites. The frequency of metabolites influenced by each of these top 50 master predictors is depicted in the bar plot shown in Figure 6. Among these genera, several have been previously linked to overall metabolite regulation in the existing literature. Below, we summarize these findings and provide master predictor rankings for the respective genera in parentheses. Davar & Zarour (2022) identified *CAG.196* and *Choladocola* (ranked 1 and 2, respectively) as key players in the microbiome’s influence on host metabolism. Notably, *CAG.196* was found to interact with a range of metabolites, including secondary bile acids and short-chain fatty acids (SCFAs), which play significant roles in immune modulation and metabolic health. The genus *Alistipes* (rank 3) has been associated with the modulation

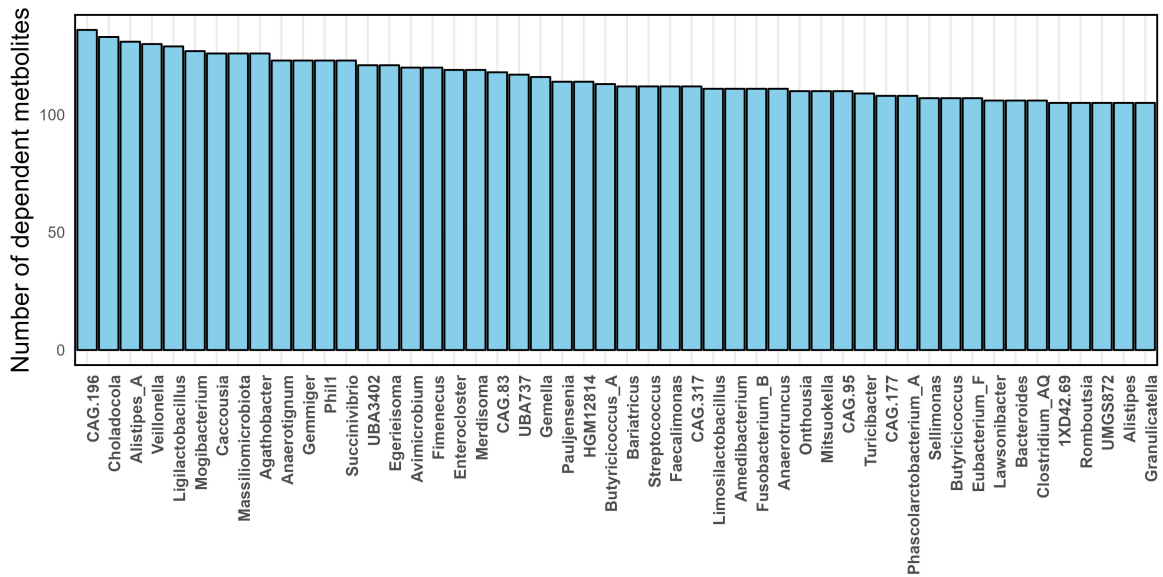


Figure 6: Bar plot depicting the frequency of metabolites influenced by each of the top 50 genera identified by B-MASTER. The plot shows the number of dependent metabolites for each genus.

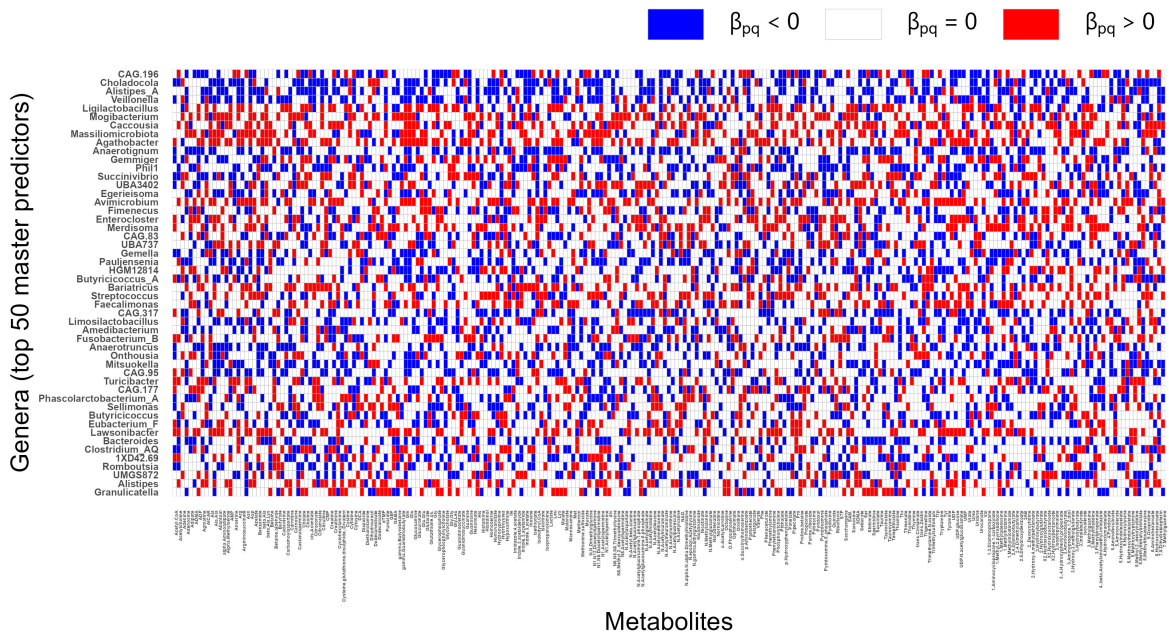


Figure 7: Heatmap illustrating the direction of the impact for each of the identified top 50 master predictors on each metabolite.

of bile acids and SCFAs, playing a pivotal role in gut-liver communication and metabolic disorders (Parker et al. 2020). Similarly, *Veillonella* (rank 4) and *Ligilactobacillus* (rank 5) are implicated in critical metabolic processes. *Veillonella* produces *propionate* from

lactate, supporting gut-liver health, while *Ligilactobacillus* is involved in lactic acid and bile salt metabolism, which enhance gut and cholesterol health (Zhang & Huang 2023). Song et al. (2022) found that *Mogibacterium* (rank 6) is associated with an increase in SCFAs, crude ash, and fat, while showing a negative correlation with amino acids in the gut. This study also highlighted *Agathobacter*, *Anaerotignum*, and *Gemmiger* (ranked 9, 10, and 11, respectively) for their roles in fiber degradation and SCFA production, both contributing to gut health and metabolic processes. Additionally, recent studies have linked *Massiliomicrobiota* (rank 8) to gut microbiota that modulate metabolic processes, including amino acid metabolism and energy production (Lu et al. 2024). Interestingly, we also note that there is limited literature available regarding the role of some of the top 50 B-MASTER-identified master predictors in overall metabolite regulation. We believe our findings offer valuable insights for biologists and clinicians, highlighting genera that may not yet be extensively studied but could play critical roles in microbiome-metabolite dynamics. In Figure 7, we present a heatmap that illustrates the direction of the impact for each of the top 50 master predictors on each metabolite.

Sub-group analyses: Apart from identifying the overall master predictor genera that influence the metabolites as a whole, we further explore the key genera that specifically impact two important subsets of metabolites. First, we focus on the list of the most abundant metabolites (as depicted in Figure 1a of Yachida et al. (2019)), and second, on the set of metabolites that were identified as differentially abundant in cancer versus control, hypothesized to be associated with the intestinal microbiota (as shown in Figure 2c of Yachida et al. (2019)). Building upon these findings, we investigate the key genera that play crucial roles in regulating these two critical subsets of metabolites. For the abundant metabolites, we consider the top 10 most prevalent compounds: *Propionate*, *Butyrate*, *Dihydrouracil*, *Glutamate*, *Urea*, *Succinate*, *5-Aminovalerate*, *Valerate*, *Lysine*, and *Alanine*, hereafter referred to as Subset 1. The set of metabolites that were differentially abundant in the cancer versus control population includes *X_DCA*, *Glycocholate*, *Taurocholate*, *Isovalerate*, *L-Isoleucine*, *L-Leucine*, *L-Valine*, *L-Phenylalanine*, *L-Tyrosine*, *L-Serine*, and *Glycine*, which we refer to as Subset 2 for the remainder of this section.

For each of these subsets, the top 15 identified master predictors (genera) were determined. The overall roles of these predictors, in terms of the direction and significance of their influence, in regulating the two subsets of metabolites are visually depicted in Fig-

ures 8 and 9, respectively. Additionally, the canonical correlation between these subsets of metabolites and the cumulatively included master predictors, arranged by their rank order, is shown in Figure 10. For Subset 1, our findings regarding *Veillonella* (rank 1) playing a key role in influencing the set of most abundant metabolites, including short-chain fatty acids (SCFAs) such as *propionate*, are consistent with similar conclusions drawn by Zhang et al. (2023). Specifically, *Veillonella* has been shown to ferment SCFAs, particularly lactate, as a source of energy, subsequently converting it into *acetate* and *propionate* (Mashima et al. 2021). This process may explain why B-MASTER identifies *Veillonella* as a significant driver behind SCFAs like *propionate*. Furthermore, *Merdicola* (rank 3) and *Mogibacterium* (rank 8) were found to influence the availability of *succinate* and other fermentation products through their involvement in carbohydrate fermentation and amino acid metabolism in the colon (Song et al. 2022). Additionally, Xu et al. (2024) observed that the genus *UBA4372* (rank 6), which is dominant in buffalo microbiomes, plays a role in immune signaling and amino acid metabolism, potentially affecting *urea* and *glutamate* synthesis.

For Subset 2, we observe a distinctive regulatory pattern in which the majority of the identified top 15 genera influence all (or most) of the differentially abundant metabolites in cancer versus control. In nearly all cases, this influence is either predominantly positive (e.g., *Ligilactobacillus*, *Faecalimonas*, *Agathobacter*, *Caccousia*, *Etepiea*, *Merdicola*) or negative (e.g., *Bacteroides*, *CAG.83*, *Anaerotignum*, *Amedibacterium*, *1XD42.69*). Yachida et al. (2019) observed that these metabolites were elevated in some or all subgroups of patients with colonoscopic findings compared to the healthy group. By connecting our findings with those of Yachida et al. (2019), we conclude that elevated levels of *Ligilactobacillus*, *Faecalimonas*, *Agathobacter*, *Caccousia*, *Etepiea*, and *Merdicola* are likely associated with increased levels of these differential metabolites, thereby being positively linked to colorectal disease progression. Conversely, elevated levels of *Bacteroides*, *CAG.83*, *Anaerotignum*, *Amedibacterium*, *1XD42.69* are negatively associated with these metabolites and are therefore more positively linked to healthy individuals. Among other findings, we identify *Gemmiger* as the most significant contributor to regulating the overall metabolite profiles in Subset 2. This genus primarily exerts a positive influence on most metabolites (hence being potentially positively associated with disease progression), while influencing *X_DCA* negatively.

Regarding the dependence mechanism between microbiome genera and these differen-

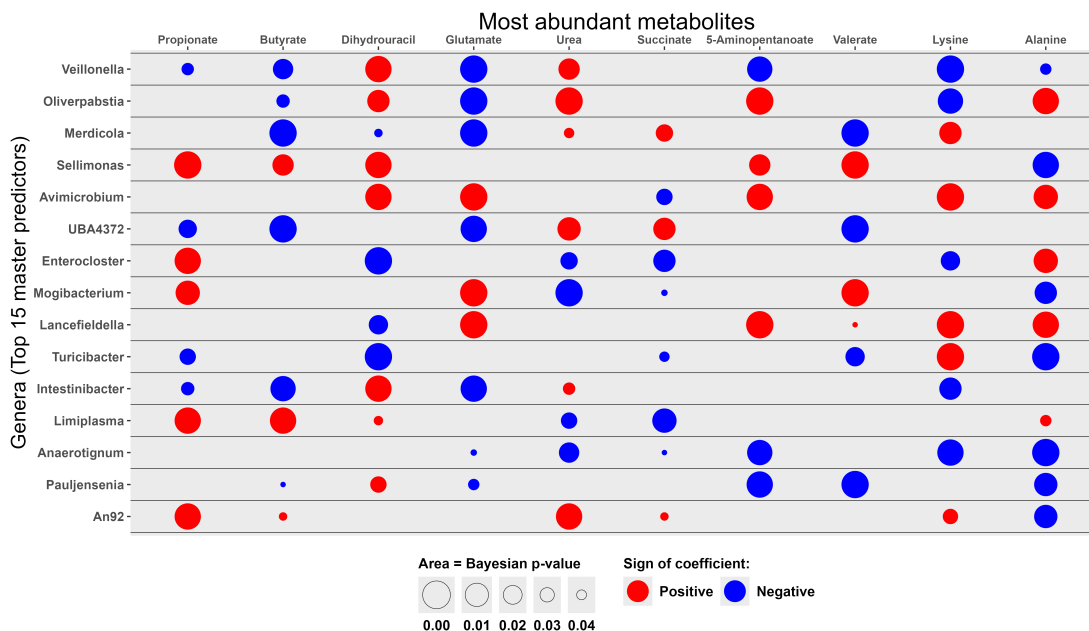


Figure 8: The plot demonstrates the direction and statistical significance of the relationships between the most abundant metabolites (Subset 1) on the corresponding top 15 key genera identified in the analysis. Progressively larger circles are associated with smaller Bayesian p-values.

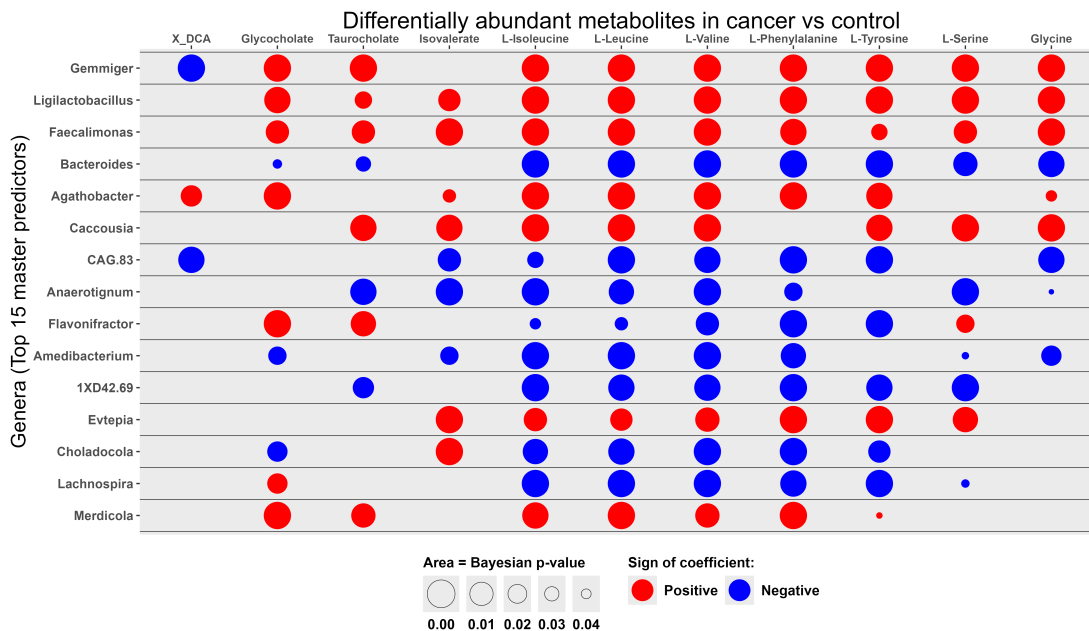


Figure 9: The plot demonstrates the direction and statistical significance of the relationships between the metabolites identified as differentially abundant in the cancer versus control comparison (Subset 2) and the top 15 key genera identified in the analysis. Progressively larger circles are associated with smaller Bayesian p-values.

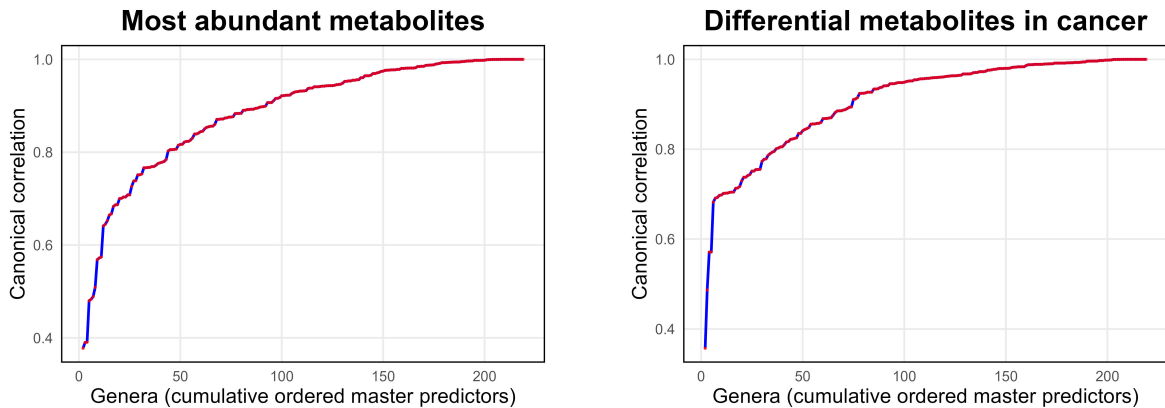


Figure 10: The canonical correlation between metabolites in Subset 1 (left) and Subset 2 (right) and the cumulatively included master predictors, arranged by their rank order, is visually depicted. The ranking of the predictors based on their prevalence is derived separately for each corresponding subset of metabolites.

tially abundant metabolites in cancer versus control, we found only a limited number of studies. Most existing literature focuses on the microbiome’s role at a higher taxonomic level, such as family, rather than genus (Dueholm et al. 2024). Furthermore, to the best of our knowledge, no existing study has directly linked the abundance levels of this specific set of genera to colorectal disease progression. Therefore, our findings provide a pioneering baseline for investigating the association between microbiome composition at the genus level and colorectal cancer progression.

Out-of-sample prediction performance study: In order to evaluate the out-of-sample prediction performance of B-MASTER relative to other existing methods, the real dataset of 220 samples is partitioned into 80% training and 20% test sets. B-MASTER, SSLASSO, mSSL, and remMap are trained on the training data. Prediction errors, specifically root mean squared error (RMSE) and mean absolute deviation (MAD), are then computed on the test data based on the estimated coefficient matrices. The results are summarized in Table 3, where B-MASTER is found to outperform the other methods.

Measures	B-MASTER	SSLASSO	mSSL	remMap
RMSE	4.556	6.047	4.619	4.623
MAD	3.327	4.937	4.208	4.216

Table 3: Out-of-sample prediction performance of B-MASTER, SSLASSO, mSSL, and remMap is evaluated by estimating the corresponding coefficient matrices using 80% of the data for training. The root-mean-squared errors (RMSE) and mean absolute deviation (MAD) are then computed on the remaining 20% of the data for testing.

5 Discussion

In this article, we present B-MASTER, a fully Bayesian approach designed to identify essential regressors within the multivariate response regression framework, complemented by a highly efficient and scalable Gibbs sampling scheme. The proposed methodology addresses several key limitations of existing approaches, as summarized below. First, the B-MASTER algorithm substantially outperforms other current methods in terms of various performance metrics, including True Positive Rate (TPR), False Positive Rate (FPR), Matthews Correlation Coefficient (MCC), Area Under the Curve (AUC), and AUC at 20% (AUC20), while maintaining a sparsity level very close to the true model. Second, B-MASTER demonstrates remarkable scalability, effectively handling high-dimensional scenarios. In contrast to the remMap and mSSL algorithms, which failed to converge within a reasonable timeframe for simulations with $P = 287, Q = 249$ (see Section 3.1), B-MASTER successfully completed model fitting in substantially less time. Additionally, its performance in extremely high-dimensional settings, including regression models with up to 4 million parameters ($P = Q = 2000$, Table 2), further underscores its scalability. Throughout all ranges of low- and high-dimensional models, B-MASTER effectively controls TPR and FPR for both independent and correlated dependent variables while maintaining reasonable computation times. Unlike existing multivariate regression methods such as remMap and mSSL, the computation time of B-MASTER remains stable and predictable as the number of predictors and response variables increases. Notably, the computation time of B-MASTER is observed to be almost invariant to sample size and consistent across datasets of the same dimension, in contrast to remMap. Finally, the computation time of B-MASTER increases linearly with the number of parameters. The robustness of B-MASTER to variations in sample size and dataset-specific attributes, coupled with its linear increase in computation time with the number of parameters, makes it exceptionally well-suited for regression tasks in ultra-high-dimensional settings. Furthermore, the predictable linear growth in computation time allows for reliable estimation of the expected runtime in advance.

Using the B-MASTER framework, we identify key components of the microbiome that influence overall metabolite profiles. Specifically, we determine the top 50 “master predictors” of gut microbiota in regulating the microbiome-metabolite dependence structure based on colorectal cancer data (Yachida et al. 2019). Furthermore, we identify a set of

key genera that influence the most abundant metabolites. Our findings align with existing studies in this area. In addition, we examine the set of genera influencing differentially abundant metabolites in cancer versus control cases. Notably, we observe a distinctive regulatory pattern where key genera consistently influence these differential metabolites either positively or negatively. Aligning our results with the findings of Yachida et al. (2019), we conclude that elevated levels of *Ligilactobacillus*, *Faecalimonas*, *Agathobacter*, *Caccousia*, *Evtapia*, and *Merdicola* are positively associated with colorectal disease progression. In contrast, healthy individuals are characterized by elevated levels of *Bacteroides*, *CAG.83*, *Anaerotignum*, *Amedibacterium*, and *1XD42.69*. This study represents the first attempt to elucidate the role of key microbiome components at the genus level potentially associated with colorectal cancer by exploring their influence on differentially abundant metabolites of colorectal cancer patients across various stages. We hope that our novel findings provide a foundational basis for further studies on modulating these identified genera as potential targets for colorectal cancer treatment or prevention in the future.

SUPPLEMENTARY MATERIAL

Supplementary text: Supplementary material is provided as a separate pdf document.

Code and data: Codes for B-MASTER, including demo, are made available on Github ([link](#)).

References

Belkaid, Y. & Hand, W. (2014), ‘Role of the microbiota in immunity and inflammation’, *Cell* **157**(1), 121–141.

Caporaso, G., Lauber, C., Walters, A. et al. (2011), ‘Global patterns of 16s rna diversity at a depth of millions of sequences per sample’, *Proceedings of the National Academy of Sciences* **108**(Supplement 1), 4516–4522.

Chakraborty, A., Bhattacharya, A. & Mallick, B. (2020), ‘Bayesian sparse multiple regression for simultaneous rank reduction and variable selection’, *Biometrika* **107**(1), 205–221.

- Chicco, D. & Jurman, G. (2020), ‘The advantages of the matthews correlation coefficient (mcc) over f1 score and accuracy in binary classification evaluation’, *BMC Genomics* **21**(6).
- Constantin, M., Chifiriuc, M., Mihaescu, G. et al. (2024), ‘Microbiome and cancer: from mechanistic implications in disease progression and treatment to development of novel antitumoral strategies’, *Frontiers in Immunology* **15**.
- Das, P., Peterson, C., Do, K. et al. (2020), ‘Bayesian simultaneous network estimation across unequal sample sizes’, *Bioinformatics* **36**(3), 798–804.
- Davar, D. & Zarour, H. (2022), ‘Facts and hopes for gut microbiota interventions in cancer immunotherapy’, *Clin. Cancer Res.* **28**(20), 4370–4384.
- Deng, L., Chen, W. & Xiao, M. (2024), ‘Metafeature selection via multivariate sparse-group lasso learning for automatic hyperparameter configuration recommendation’, *IEEE Transactions on Neural Networks and Learning Systems* **35**(9), 12540–12552.
- Deshpande, S., Rockova, V. & George, E. (2019), ‘Simultaneous variable and covariance selection with the multivariate spikeand-slab lasso’, *Journal of Computational and Graphical Statistics* **28**(4), 921–931.
- Dueholm, M., Andersen, K., Korntved, A. et al. (2024), ‘Midas 5: Global diversity of bacteria and archaea in anaerobic digesters’, *Nature Communications* **15**(5361).
- Fan, J. & Li, R. (2001), ‘Variable selection via nonconcave penalized likelihood and its oracle properties’, *Journal of the American Statistical Association* **96**(456), 1348–1360.
- Feng, Q., Liang, S., Jia, H. et al. (2015), ‘Gut microbiome development along the colorectal adenoma-carcinoma sequence’, *Nature Communications* **6**, 6528.
- Friedman, J., Hastie, T. & Tibshirani, R. (n.d.), ‘Regularized paths for generalized linear models via coordinate descent’, *Technical report, Dept. Statistics, Stanford Univ.*
- Garrett, S. (2015), ‘Cancer and the microbiota’, *Science* **348**(6230), 80–86.
- Goh, G., Dey, D. & Chen, K. (2017), ‘Bayesian sparse reduced rank multivariate regression’, *Journal of Multivariate Analysis* **157**, 14–28.

- Hoerl, A. & Kennard, R. (1970), ‘Ridge regression: Biased estimation for nonorthogonal problems’, *Technometrics* **12**(1).
- Huse, S., Welch, D., Morrison, G. et al. (2008), ‘Exploring microbial diversity and taxonomy using ssu rna hypervariable tag sequencing’, *PLoS Genetics* **4**(11), e1000255.
- Jobin, C. (2018), ‘Precision medicine using microbiota’, *Science* **359**(6371), 32–34.
- Kyung, M., Gill, J. & Ghosh, M. (2010), ‘Penalized regression, standard errors, and bayesian lassos’, *Bayesian Analysis* **5**(2), 369–411.
- Lederberg, J. & McCray, A. (2001), ‘“ome sweet” omics: A genealogical treasury of words’, *The Scientist* **15**(7), 8.
- Li, H. (2015), ‘Microbiome, metagenomics, and high-dimensional compositional data analysis’, *Annual Review of Statistics and Its Application* **2**, 73–94.
- Li, Y., Nan, B. & Zhu, J. (2015), ‘Multivariate sparse group lasso for the multivariate multiple linear regression with an arbitrary group structure’, *Biometrics* **71**(2), 354–363.
- Liquet, B., Mengersen, K., Pettitt, A. et al. (2017), ‘Bayesian variable selection regression of multivariate responses for group data’, *Bayesian Analysis* **12**(4), 1039–1067.
- Liu, J., Tan, Y., Cheng, H. et al. (2022), ‘Functions of gut microbiota metabolites, current status and future perspectives’, *Aging and Disease* **13**(4), 1106–1126.
- Lu, Y., Hui, F., Zhou, G. et al. (2024), ‘Microbiomenet: exploring microbial associations and metabolic profiles for mechanistic insights’, *Nucleic Acids Research* **gkae944**, 1–8.
- Lu, Y., Yuan, X., Wang, M. et al. (2022), ‘Gut microbiota influence immunotherapy responses: mechanisms and therapeutic strategies’, *Journal of Hematology & Oncology* **15**(47).
- Malczewski, A., Navarro, S., Coward, J. et al. (2020), ‘Microbiome-derived metabolome as a potential predictor of response to cancer immunotherapy’, *Journal for ImmunoTherapy of Cancer* **8**, e001383.
- Mashima, I., Liao, Y., Lin, C. et al. (2021), ‘Comparative pan-genome analysis of oral veillonella species’, *Microorganisms* **9**(8).

- MathWorks (2024), ‘Quick start parallel computing in matlab’. Accessed: 2024-11-19.
URL: <https://www.mathworks.com/help/parallel-computing/>
- Muller, E., Algavi, Y. & Borenstein, E. (2022), ‘The gut microbiome-metabolome dataset collection: a curated resource for integrative meta-analysis’, *npj Biofilms and Microbiomes* **8**(1), 79.
- Park, T. & Casella, G. (2008), ‘The bayesian lasso’, *Journal of the American Statistical Association* **103**(482), 681–686.
- Parker, B., Wearsch, P., Veloo, A. et al. (2020), ‘The genus alistipes: Gut bacteria with emerging implications to inflammation, cancer, and mental health’, *Mental Health. Front. Immunol.* **11**(906).
- Peng, J., Wang, P., Zhou, N. et al. (2009), ‘Partial correlation estimation by joint sparse regression models’, *Journal of the American Statistical Association* **104**(486), 735–746.
- Peng, J., Zhu, J., Bergamaschi, A. et al. (2010), ‘Regularized multivariate regression for identifying master predictors with application to integrative genomics study of breast cancer’, *Annals of Applied Statistics* **4**(1), 53–77.
- Qian, J., Taigawa, Y., Du, W. et al. (2020), ‘A fast and scalable framework for large-scale and ultrahigh-dimensional sparse regression with application to the uk biobank’, *PLoS Genetics* **16**(10), e1009141.
- Rockova, V. & George, E. (2018), ‘The spike-and-slab lasso’, *Journal of the American Statistical Association* **113**(521), 431–444.
- Roy, V. & Chakraborty, S. (2017), ‘Selection of tuning parameters, solution paths, and standard errors for bayesian lassos’, *Bayesian Analysis* **12**(3), 753–778.
- Schwarz, G. (1978), ‘Estimating the dimension of a model’, *Annals of Statistics* **6**(2), 461–464.
- Shokralla, S., Spall, J., Gibson, J. et al. (2012), ‘Next-generation sequencing technologies for environmental dna research’, *Molecular Ecology* **21**(8), 1794–1805.

- Song, Y., Chen, K., Lv, L. et al. (2022), ‘Uncovering the biogeography of the microbial community and its association with nutrient metabolism in the intestinal tract using a pig model’, *Front. Nutr.* **9**(1003763).
- Tibshirani, R. (1996), ‘Regression shrinkage and selection via the Lasso’, *Journal of the Royal Statistical Society: Series B (Statistical Methodology)* **58**(1), 267–288.
- Visconti, A., LeRoy, C., Rosa, F. et al. (2019), ‘Interplay between the human gut microbiome and host metabolism’, *Nature Communications* **10**(1), 1–10.
- Wang, L. & Ganly, I. (2017), ‘The oral microbiome and oral cancer’, *Clinical Laboratory Medicine* **37**(4), 425–441.
- Xia, Y. & Sun, J. (2017), ‘Hypothesis testing and statistical analysis of microbiome’, *Genes & Diseases* **4**(3), 138–148.
- Xu, X. & Ghosh, M. (2015), ‘Bayesian variable selection and estimation for group lasso’, *Bayesian Analysis* **10**(4), 909–936.
- Xu, Y., Feng, T., Ding, Z. et al. (2024), ‘Age-related compositional and functional changes in the adult and breastfed buffalo rumen microbiome’, *Frontiers in Microbiology* **15**.
- Xu, Z. & Knight, R. (2015), ‘Dietary effects on human gut microbiome diversity’, *British Journal of Nutrition* **113**(S1), S1–S5.
- Yachida, S., Mizutani, S., Shiroma, H. et al. (2019), ‘Metagenomic and metabolomic analyses reveal distinct stage-specific phenotypes of the gut microbiota in colorectal cancer’, *Nature Medicine* **25**(6), 968–976.
- Yang, W. & Cong, Y. (2021), ‘Gut microbiota-derived metabolites in the regulation of host immune responses and immune-related inflammatory diseases’, *Cellular & Molecular Immunology* **18**(4), 866–877.
- Yuan, M. & Lin, Y. (2006), ‘Model selection and estimation in regression with grouped variables’, *Journal of the Royal Statistical Society: Series B (Statistical Methodology)* **68**(1), 49–67.

- Zhang, L., Zi, L., Kuang, T. et al. (2023), ‘Investigating causal associations among gut microbiota, metabolites, and liver diseases: a mendelian randomization study’, *Front. Endocrinol.* **14**(1159148).
- Zhang, S. & Huang, S. (2023), ‘The commensal anaerobe veillonella dispar reprograms its lactate metabolism and short-chain fatty acid production during the stationary phase’, *Microbiology Spectrum* **11**(2), e03558–22.
- Zhang, W., An, Y., Qin, X. et al. (2021), ‘Gut microbiota-derived metabolites in colorectal cancer: the bad and the challenges’, *Frontiers in Oncology* **11**, 739648.
- Zou, H. (2006), ‘The adaptive lasso and its oracle properties’, *Journal of the American Statistical Association* **101**(476), 1418–1429.
- Zou, H. & Hastie, T. (2005), ‘Regularization and variable selection via the elastic net’, *Journal of the Royal Statistical Society: Series B (Statistical Methodology)* **67**(2), 301–320.